Manifestations of Electronic Correlations in the Diffraction of Electron Pairs from Crystals

J. Berakdar,* S. N. Samarin, R. Herrmann, and J. Kirschner
Max-Planck-Institut für Mikrostrukturphysik, Weinberg 2, 06120 Halle, Germany
(Received 23 March 1998)

The energy-sharing spectra of correlated electron pairs ejected from Cu(001) and Fe(110) surfaces reveal characteristic structures associated with diffraction of the pair from the lattice. It is demonstrated theoretically and experimentally that (1) the momentum-space *positions* of these new features are determined by the change of the center-of-mass wave vector of the pairs as compared to the reciprocal lattice vector, and (2) the relative *intensities* of the peaks and the *shapes* of the individual peaks are dependent on the internal correlation of the pairs. Possible pathways for the pair creation are envisaged at various diffracted beams. [S0031-9007(98)07432-8]

PACS numbers: 79.20.Kz

An electronic system distorted externally by a photon or a charged particle impact can integrally respond by the simultaneous emission of two electrons into the vacuum. The vacuum states of these two correlated electrons can be then determined using an angular and energy-resolved coincidence technique. The spectra of low-energy electron pairs, the subject of this study, carry the signature of their mutual correlations and their coupling to other degrees of freedom of the environment while in the high energy regime information on the initial-momentum components of the pair can be extracted from the recorded spectra [1–4]. These observations have been made in diverse areas of physics, such as plasma, atomic, molecular, and condensed matter physics [3,5,6]. For pair emission from localized electronic states, such as atomic and molecular orbitals, it turns out that the spectra are dominated by the interelectronic interaction of the pair, in particular at lower energies (with respect to the initial orbital energies) [6]. Thus, an adequate theoretical description of these phenomena must go beyond an independent particle description. For delocalized electronic states, as present in metallic crystals and surfaces, it is established that delocalization does not preclude correlations. E.g., in transition metals the *d* electrons are delocalized, yet correlation between them is far from weak.

In this work it is shown theoretically and experimentally that an electron pair can be regarded as a "two-electron quasiparticle." The scattering of this quasi-single-particle from a crystal potential results in characteristic diffraction pattern that is, for the first time, experimentally observed. The positions of the diffraction peaks are governed by a von Laue–like diffraction condition for the center-of-mass wave vector of the electron pair. The relative intensities of the diffraction maxima are largely determined by the internal degree of freedom of the pair, i.e., by interelectronic correlations.

The experimental setup used for the angular and energy-resolved detection of the pairs, i.e., for the projection of the two-electron initial state onto the two-electron vacuum state, is schematically depicted in Fig. 1. A more detailed description can be found in Refs. [7–9]. The sample surface defines the x-y plane, while the z axis coincides with the surface normal. In the z-x plane two position sensitive microchannel plate electron detectors are located at a distance of 160 mm to the sample surface, such that the relative angle between the detector axes and the surface normal is given by $\pm\alpha$. The angular acceptance of each electron detector within the scattering plane is $\pm 13.2°$. A parallel electron beam of about 1 mm diameter impinges onto the sample surface including the angle γ with the surface normal. For investigating the Cu(001) sample, the angles α and γ are chosen to be 40° and 0°, respectively, while in the case of Fe(110) (BCC), α was set to be 50° and $\gamma = 5°$. Correlated electron pairs emitted from the sample upon excitation by a primary electron are detected in coincidence. Their energies have been measured using a time-of-flight technique. In the range of electron energies detected here, we achieve an energy resolution of $\Delta E = 0.4–0.8$ eV. Standard cleaning procedure of the surface is applied before each measurement under a base pressure in the range of 10^{-11} mbar.

The probability for the two electrons to be detected with asymptotic momenta $\mathbf{k}_1$ and $\mathbf{k}_2$ is derived from an

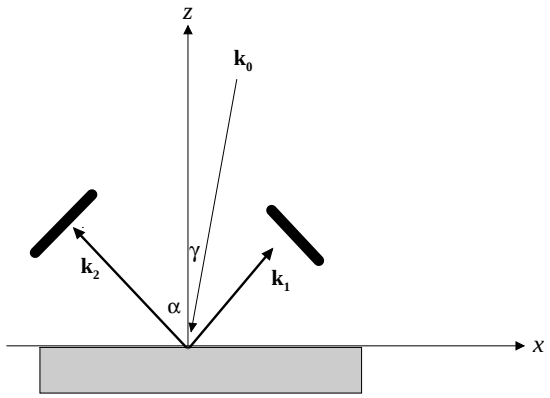

FIG. 1. A schematic representation of the experimental setup as described in the text.

excitation amplitude, $\mathcal{T}$, that is, to leading order, a sum of direct electron pair excitation amplitude, T_{ee}, and an amplitude, T_{ec}, that involves the scattering of the pair from the crystal potential W_{ec} [10,11] (i.e., atomic units [a.u.] are used throughout)

$$\mathcal{T} = T_{ee} + T_{ec}. \tag{1}$$

To emphasize the quasi-single-particle nature of the correlated pair we canonically transform to a wave vector representation $\mathbf{K}^- \otimes \mathbf{K}^+$ where $\mathbf{K}^+ = \mathbf{k}_1 + \mathbf{k}_2$ is the center-of-mass wave vector of the pair, and $\mathbf{K}^- = (\mathbf{k}_1 - \mathbf{k}_2)/2$ characterizes the interelectronic wave vector, i.e., the internal degree of freedom of the pair. The direct pair emission amplitude has the form

$$T_{ee} = \langle \mathbf{K}^-, \mathbf{K}^+ | W_{ee} | \mathbf{k}_0, \chi_{\epsilon(\mathbf{k})} \rangle, \tag{2}$$

where $|\mathbf{k}_0, \chi_{\epsilon(\mathbf{k})}\rangle$ is the state vector describing the pair as initially prepared by the experiment. In the present work $|\mathbf{k}_0, \chi_{\epsilon(\mathbf{k})}\rangle$ consists of an excited electronic vacuum state with wave vector $\mathbf{k}_0$ and a bound state $|\chi_{\epsilon(\mathbf{k})}\rangle$ with energy ϵ and wave vector $\mathbf{k}$. These two states are then coupled via a screened (renormalized) Coulomb interaction W_{ee}. The transition amplitude T_{ec} that describes scattering from the semi-infinite crystal can be deduced to

$$T_{ec} = \iint d^3\mathbf{p}\, d^3\mathbf{q} \langle \mathbf{K}^-, \mathbf{K}^+ | W_{ee} g_{ee}^- | \mathbf{p}, \mathbf{q} \rangle \times \langle \mathbf{p} | W_{ec} | \mathbf{k}_0 \rangle \langle \mathbf{q} | \chi_{\epsilon(\mathbf{k})} \rangle. \tag{3}$$

Here g_{ee}^- is the propagator in the interelectronic Coulomb interaction, W_{ec} is the interaction potential between the projectile and the lattice, and $|\mathbf{q}\rangle \otimes |\mathbf{p}\rangle$ is a complete set of plane waves. For the numerical calculations presented here we approximate W_{ec} by nonoverlapping muffin-tin ionic potentials V^{ion} ($W_{ec} = \sum_i V_i^{\text{ion}}$). The quality of this approximation is discussed in Ref. [12]. The form factor $\tilde{W}_{ec} := \langle \mathbf{p} | W_{ec} | \mathbf{k}_0 \rangle$ can then be reduced to

$$\tilde{W}_{ec} = \frac{N\sqrt{2\pi} f}{A_{uc}} \sum_{\ell} e^{-iK_z r_{\perp,\ell}} \sum_{\mathbf{g}_\parallel} \delta^{(2)}(\mathbf{g}_\parallel - \mathbf{K}_\parallel) \tilde{V}^{\text{ion}}(\mathbf{K}). \tag{4}$$

In Eq. (4) $\tilde{V}^{\text{ion}}(\mathbf{K})$ is the Fourier transform of V^{ion}, N is the number of ionic cores illuminated by the electron beam, A_{uc} is the volume of the two-dimensional unit cell, $\mathbf{g}_\parallel$ is the surface reciprocal lattice vector, ℓ enumerates the atomic layers with shortest distance $r_{\perp,\ell}$ with respect to the origin, $\mathbf{K} = \mathbf{p} - \mathbf{k}_0$, and $f = \exp(i\mathbf{p} \cdot \mathbf{r}_1)$ with $\mathbf{r}_1$ referring to the position of the bound electron.

The decisive point is that due to Bloch's theorem, which relies only on the two-dimensional periodicity of W_{ec}, regardless of it's actual functional form, the transition amplitudes T_{ec} and T_{ee} can be expressed as

$$T_{ec} = C \sum_{\ell, \mathbf{g}_\parallel} \delta^{(2)}[\mathbf{g}_\parallel - (\mathbf{K}_\parallel^+ - \mathbf{K}_{0,\parallel})] \times \mathcal{L}(\mathbf{g}_\parallel, \ell, \mathbf{K}^+, \mathbf{K}^-, \mathbf{k}), \tag{5}$$

whereas T_{ee} is given by

$$T_{ee} = \delta^{(2)}(\mathbf{K}_{0,\parallel} - \mathbf{K}_\parallel^+)\, \mathcal{L}'. \tag{6}$$

In Eq. (6) $\mathbf{K}_0 = \mathbf{k}_0 + \mathbf{k}$ is the initial wave vector of the pair. The functions $C, \mathcal{L}, \mathcal{L}'$ depend on the description of the momentum-space wave function $\langle \mathbf{q} | \chi_{\epsilon(\mathbf{k})} \rangle$ of the bound electron. For a jellium-state momentum distribution and free interelectronic propagation, Eqs. (5) and (6) can be evaluated in closed form [10].

Equation (5) has important implications:

(1) Only the pair center-of-mass wave vector enters in the von Laue-like diffraction condition, expressed by the delta function. This is equivalent to a diffraction of a quasiparticle located at the pair's center of mass when the parallel component of its wave vector is changed by $\mathbf{g}_\parallel$ during the collision. We note that in LEED studies (Low Energy Electron Diffraction) diffraction occurs when the change in the wave vector of the incident electron equals $\mathbf{g}_\parallel$ [12,13]. The decisive difference to the pair's diffraction is that a fixed $\mathbf{K}^+$ does not imply fixed $\mathbf{k}_1, \mathbf{k}_2$ since a momentum exchange of the two electrons (the internal coordinate $\mathbf{K}^-$ changes then) does not necessarily modify $\mathbf{K}^+$. Therefore, a definite change in $\mathbf{K}^+$ does not fix the amount of change in the wave vector of the incoming projectile.

(2) While $\mathbf{K}^+$ determines the *positions* of the diffraction peaks, the functional dependence of $\mathcal{L}$ on $\mathbf{K}^-$, which characterizes the strength of electronic correlations (in momentum space W_{ee} depends only on $|\mathbf{K}^-|$), controls the *intensity* of the individual diffraction peaks. Furthermore, the *shape* of the individual peaks is influenced by the interelectronic correlation.

(3) The distribution of the wave vector $\mathbf{k}_\parallel$ of the initially bound Bloch electron results in a smear-out effect of the diffraction pattern even in the case where $\mathbf{K}^+$ and $\mathbf{k}_0$ are experimentally sharply resolved.

(4) Conversely, in case $\mathbf{K}_\parallel^+, \mathbf{g}_\parallel$ and $\mathbf{k}_{0,\parallel}$ are well defined, the position and widths of the diffraction peaks reflects the character of $\mathbf{k}_\parallel$.

To substantiate the above statements we performed, using the setup depicted in Fig. 1, three sets of measurements where, for a fixed incident E_i and total excess energies $E_{\text{tot}} = (k_1^2 + k_2^2)/2$ of the pair, we scan the electrons' energy sharing. As shown in Fig. 1, $\mathbf{k}_0, \mathbf{k}_1, \mathbf{k}_2$ lie in the x-z plane, i.e., $\mathbf{K}_\parallel^+$ possesses only one nonvanishing component K_x^+ along the x axis. As indicated above, it is this component that is relevant for the pair diffraction, and hence we investigate the energy sharing as function of K_x^+. Since $E_{\text{tot}} = K^{+^2}/2m + K^{-^2}/2m_\mu$, where $m = 2$ is the total mass of the pair and $m_\mu = 0.5$ is their reduced mass, the value of K_x^+ is generally restricted to $0 \le K_x^+ \le \sqrt{4E_{\text{tot}}}$. In the arrangement of Fig. 1 the condition

$$-\sin\alpha \sqrt{2E_{\text{tot}}} \le K_x^+ \le \sin\alpha \sqrt{2E_{\text{tot}}} \tag{7}$$

has to be imposed. In Fig. 2 the results are presented for a Cu(001) monocrystal. The cross section is then proportional to $|\mathcal{T}|^2$ [Eq. (1)]. An integration over $\mathbf{k}_\parallel$ (weighted

with the density of states) is, however, necessary as it is not experimentally resolved [10]. Furthermore, an average of the spin degrees of freedom has been performed.

Since $\gamma = 0$ in Fig. 2, the whole experimental arrangement, i.e., the scattering plane, spanned by $\mathbf{k}_1$ and $\mathbf{k}_2$, and the crystal is invariant under 180° rotation around $\hat{\mathbf{z}}$ (note that $\mathbf{k}_0 \parallel \hat{\mathbf{z}}$ lies in the scattering plane and is the bisector of the relative angle $\cos^{-1} \hat{\mathbf{k}}_1 \cdot \hat{\mathbf{k}}_2$). Thus, the spectrum depicted in Fig. 2 is symmetric with respect to $K_x^+ = 0$. Furthermore $\mathcal{L}$, $\mathcal{L}'$ are symmetric with respect to $K_x^+ = 0$; hence structures left and right to $K_x^+ = 0$ are modified in the same way by $\mathcal{L}$, $\mathcal{L}'$.

For illustration, assuming $\mathbf{k}_\parallel = 0$, the positions of the first diffraction maxima [hereafter referred to as the $(-1,0)$ $(1,0)$ maxima] are indicated by arrows. The theoretical and experimental data (Fig. 2) clearly show the onset of the $(1,0)$, and $(-1,0)$ diffraction peaks. The abrupt decrease of these peaks at the wings is due to the cutoff condition (7). The structure in the middle is due to the specular beam $(0,0)$. This is clearly demonstrated by analyzing separately the contributions $|T_{ee}|$ and $|T_{ec}|$ to the total transition amplitude (1). By far the major contribution originates from T_{ec} [Eq. (5)], i.e., from events where the pair is back-reflected from the crystal potential. Nonetheless, at the specular beam the amplitude T_{ee} [Eq. (6)] provides an observable contribution to the total transition amplitude $|\mathcal{T}| = |T_{ec} + T_{ee}|$ (cf. Fig. 2). The contribution of $|T_{ee}|$ [Eq. (6)] to the $(-1,0)$ and $(1,0)$ peaks vanishes identically. This is in line with Eq. (6) and supports the identification of these peaks as $(-1,0)$ and $(1,0)$ diffraction maxima of the pair. As suggested above, the width of the structure corresponding to the $(0,0)$ diffraction is determined by the initial momentum components of the pair. Since k_0 is fixed by the experiment, the initial momentum distribution of the pair is given by that of the bound electron with its maximum value being the Fermi wave vector k_F. I.e., each of the diffraction peaks has an extension of $K_x^+ = \pm k_F$. This is consistent with the experimental findings of Figs. 2–4. We note however, that the cutoff condition (7) has to be superimposed on the widths of the diffraction peaks, in particular on those at the wings of the spectra.

Going down with E_{tot} (and E_i) the variation interval of K_x^+ shrinks according to Eq. (7). In fact, at $E_i = 34$ eV and $E_{\text{tot}} = 27$ eV (see Fig. 3) only the structure in the middle of Fig. 2 is captured by the region in which K_x^+ is allowed. To demonstrate the sensitivity of the spectra

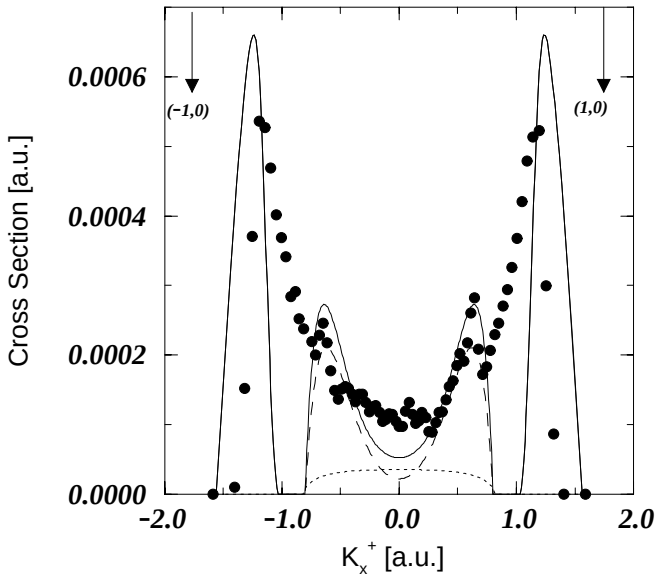

FIG. 2. For a fixed incident energy $E_i = 85$ eV and fixed excess energy $E_{\text{tot}} = 79$ eV, the excess energy-sharing of the escaping electrons is depicted as function of $K_x^+ = k_{1,x} + k_{2,x}$. The experiment has been performed on a Cu(001) crystal in normal incidence, corresponding to $\gamma = 0$ in Fig. 1, Furthermore, we choose $\alpha = 40°$ (cf. Fig. 1). Depicted are the separate contributions of amplitudes for direct pair emission [$|T_{ee}|$ as given by Eq. (6)] (dotted curve) and the amplitude for the pair's scattering from the lattice potential [$|T_{ec}|$ as defined by Eq. (5)] (dashed curve). Calculations using the coherent sum $|\mathcal{T}| = |T_{ee} + T_{ec}|$ (solid curve) are also shown. The calculations are performed for infinite energy and angular resolution of the detectors; for clarity the theoretical $(-1,0)$ and $(1,0)$ diffracted peaks are scaled down by 2. The positions of the $(1,0)$ and $(-1,0)$ diffracted beams are indicated (see text). The experimental data (full dots) are on relative scale.

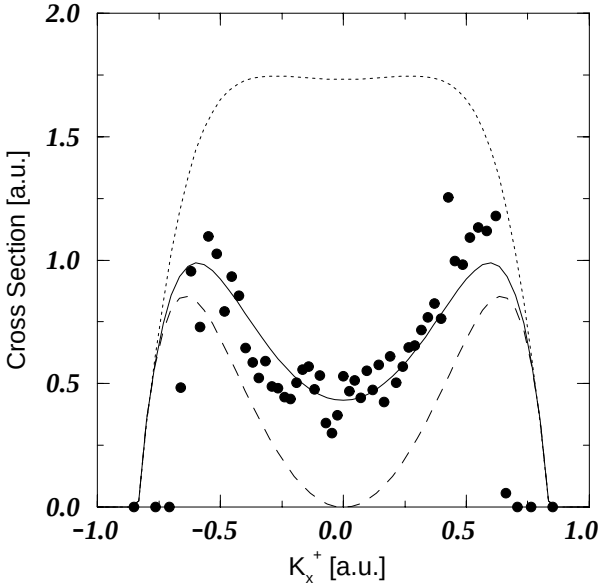

FIG. 3. The same as in Fig. 2, however, the incident energy is lowered to $E_i = 34$ eV and $E_{\text{tot}} = 27$ eV. For the calculations we employ the coherent sum, $\mathcal{T}$, of the amplitudes for the direct pair emission and the pair's scattering from the crystal potential, i.e., $\mathcal{T} = T_{ee} + T_{ec}$ [Eq. (1)]. The singlet σ^s (dotted curve) and the triplet σ^t (dashed curve) scattering cross sections are shown along with their statistical average, $0.25\sigma^s + 0.75\sigma^t$ (solid curve). The finite experimental resolution has not been taken into account. The spin nonresolved experimental data (full dots) are relative and have been normalized to theory at one point.

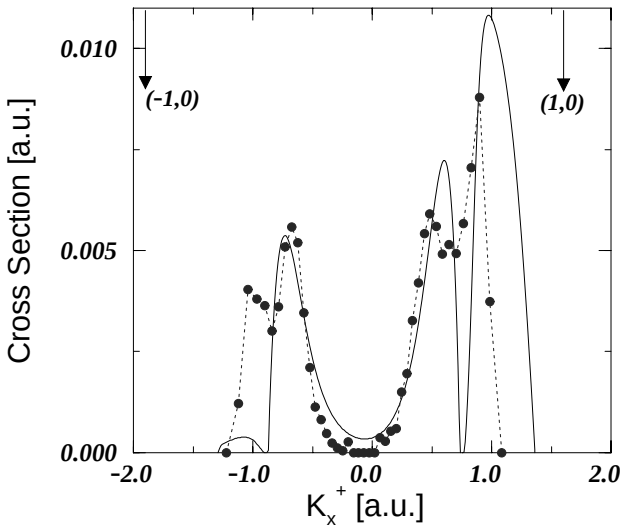

Fig. 4. The experimental results (full dots) for a Fe(110) (BCC) sample at an incident energy of 50 eV and $E_{\mathrm{tot}} = 44$ eV. The incident beam is tilted with respect to the normal by an angle of $\gamma = 5°$ and $\alpha = 50°$ (cf. Fig. 1). Theoretical results (solid curve) are obtained by evaluating $|\mathcal{T}| = |T_{ee} + T_{ec}|$ [Eq. (1)].

to the interelectronic coupling we investigate the singlet (dotted curve in Fig. 3) and the triplet (dashed curve in Fig. 3) scattering contribution to the spin nonresolved spectrum (solid curve in Fig. 3). Because of symmetry requirement the triplet scattering must vanish when the two electron emerge with the same energies, i.e., for $K_x^+ = 0$. In fact, inspecting Fig. 3 we can deduce that the minimum in the spin-averaged spectrum around $K_x^+ = 0$ is primarily due to the diminishing triplet contribution at $K_x^+ = 0$. The same has been observed for the cases of Figs. 2 and 4. Further investigations (not shown here for space limitations) have shown that the absolute magnitude of the spectra is strongly dependent on the amount of screening of the interelectronic Coulomb interaction.

In the last example (Fig. 4) performed for Fe(110) the crystal and the scattering plane do not have a common symmetry axis. This is reflected in a break of symmetry of the spectra. The initial wave-vector distribution of the pair $K_{0,x}$ is then modified in a preferential direction determined by $k_{0,x} = 0.17$ a.u. This is of prime importance when determining the change of the wave vector of the pair during the collision that in turn decides the diffraction pattern. E.g., the positions of the $(-1, 0)$ and $(1, 0)$ diffraction peaks in Fig. 4 are not symmetric with respect to $K_x^+ = 0$, in contrast to Figs. 2 and 3. Hence, only a reminiscence of $(-1, 0)$ diffraction is seen in the spectra shown in Fig. 4. An interplay of this effect with the scattering dynamics, described by the now asymmetric functions $\mathcal{L}, \mathcal{L}'$ in Eqs. (5) and (6), leads to the relative heights of the peaks as observed in Fig. 4.

From an analysis, analogous to that done in Fig. 2, we conclude in cases of Figs. 3 and 4 that pair emission at the $(-1, 0)$ and $(1, 0)$ beams is solely due to the amplitude T_{ec} Eq. (5). The pair generation around the specular beam $(0, 0)$ is dominated by (5) as well, however, interference with the amplitude T_{ee} [Eq. (6)] is evident. Investigating the sum over ℓ in Eq. (5) we deduce that in this present case of Figs. 2–4 correlated pairs are predominantly generated in the two topmost atomic layers.

*Email Address: jber@mpi-halle.de

[1] I. E. McCarthy and E. Weigold, Rep. Prog. Phys. **54**, 789 (1991).
[2] M. A. Coplan, J. H. Moore, and J. P. Doering, Rev. Mod. Phys. **66**, 98 (1994).
[3] M. Vos and I. E. McCarthy, Rev. Mod. Phys. **67**, 713 (1995).
[4] A. S. Kheifets, S. Iacobucci, A. Ruoccoa, R. Camilloni, and G. Stefani, Phys. Rev. B **57**, 7360 (1998).
[5] *Electron Impact Ionization*, edited by T. D. Mark and G. H. Dunn (Springer-Verlag, Vienna, 1985).
[6] *Coincidence Studies of Electron and Photon Impact Ionization*, edited by C. T. Whelan and H. R. J. Walters (Plenum Press, New York, London, 1997), and references therein.
[7] J. Kirschner, O. M. Artamonov, and A. N. Terekhov, Phys. Rev. Lett. **69**, 1711 (1992).
[8] J. Kirschner, O. M. Artamonov, and S. N. Samarin, Phys. Rev. Lett. **75**, 2424 (1995).
[9] O. M. Artamonov, S. N. Samarin, and J. Kirschner, Appl. Phys. A **65**, 535 (1997).
[10] J. Berakdar and M. P. Das, Phys. Rev. A **56**, 1403 (1997).
[11] H. Gollisch, G. Meinert, Xiao Yi, and R. Feder, Solid State Commun. **102**, 317 (1997).
[12] J. B. Pendry, *Low Energy Electron Diffraction* (Academic Press, London, 1974).
[13] M. A. van Hove, W. H. Weinberg, and C.-M. Chan, *Low Energy Electron Diffraction*, in Springer Series in Surface Science (Springer, Berlin, 1986).